CO2 IR radiation modelling with a multi-temperature approach in flows under vibrational nonequilibrium

Quentin Binauld, Philippe Rivière, Jean-Michel Lamet, Lionel Tessé, Anouar Soufiani

CO_2 IR radiation modelling with a multi-temperature approach in flows under vibrational nonequilibrium

Quentin Binauld[a,b], Philippe Rivière[a,*], Jean-Michel Lamet[b], Lionel Tessé[b], Anouar Soufiani[a]

[a] *Laboratoire EM2C, CNRS, CentraleSupélec, Université Paris Saclay, 3 rue Joliot Curie, 91192 Gif-sur-Yvette Cedex, France*
[b] *ONERA/DMPE, Université de Toulouse, F-31055, Toulouse, France*

Abstract

The aim of this paper is to develop a line by line model for CO_2 vibrational nonequilibrium radiation and to investigate nonequilibrium effects in the case of some applications involving high temperature expanding flows. A vibrational specific collisional relaxation model is developed and is incorporated in a multi-temperature thermodynamic description of the gas mixture, in order to compute vibrational level populations along the flow. The HITEMP-2010 spectroscopic database is employed with a model for level energy splitting to provide line by line absorption and emission total and per-vibrational mode specific spectra. The specific spectra allow us to derive the radiative source terms to be used in the multi-temperature model if a coupled approach is required. The model is applied first to a simple conical nozzle flow and then to the plume of a high altitude solid propellant rocket engine. It is shown that, for the considered applications, the partial freeze of vibrational excitation in the expanding flow increases significantly the radiative intensity escaping

*Corresponding author.
Email address: philippe.riviere@centralesupelec.fr (Philippe Rivière)

from the mixture.

Keywords: CO_2 radiation, Vibrational nonequilibrium, Multi-temperature model, Expanding jets

---

1. Introduction

Departure from Local Thermodynamic Equilibrium (LTE) in gases occurs when internal relaxation time scales become comparable or higher than hydrodynamic time scales. The resulting Non-Local Thermodynamic Equilibrium (NLTE) state may be characterized by an excess of vibrational energy as compared to translational energy in the case for instance of expanding flows like rocket plumes at high altitudes [1]. On the contrary, for compressed or shocked flows like those facing Martian atmospheric entry vehicles, the kinetic energy is first transformed into translational energy and vibrational excitation is delayed compared to translation and rotation [2]. In the above mentioned applications CO_2 is among the main contributing gaseous species to radiative transfer. CO_2 NLTE radiation is also an important mechanism in many other fields including electrically excited [3] and gas dynamic [4] CO_2 lasers, and radiative transfer in the upper layers of Earth atmosphere [5]. For these two latter applications, several models have been developed in the past but they only involve low-lying vibrational states of CO_2 (see e.g. [6]).

Modelling radiative transfer under NLTE conditions remains a challenging task. It requires, in addition to accurate spectroscopic data and radiation solver, the knowledge of the local population of each rovibrational level, which can be determined from a vibrational kinetic model associated with either

a detailed state-to-state model or with a multi-temperature model (see e.g. [7]). The main goal of this paper is to develop such a radiative transfer model for CO_2 (Sec. 2), based on HITEMP-2010 spectroscopic database [8] and a multi-temperature level population model (Sec. 3). The model is applied in Sec. 4 to a simple expanding supersonic nozzle flow to quantify NLTE effects in this application. Then, the model is applied in Sec. 5 to the case of a high altitude plume of a solid propellant rocket. In the multi-temperature model developed here, CO_2 translational and rotational modes are assumed to be at local equilibrium and are described by a single temperature T due to the fast translation-rotation exchanges. Vibrational levels are assumed to follow a Boltzmann distribution at a single temperature T_{12} for the symmetric stretching mode ($\nu_1 \simeq 1388$ cm^{-1}) and the two-fold degenerate bending mode ($\nu_2 \simeq 667$ cm^{-1}), due to Fermi Resonance [9], and a Boltzmann distribution at a different temperature T_3 for the antisymmetric stretching mode ($\nu_3 \simeq 2349$ cm^{-1}). Although some CFD models are based on a single vibrational temperature (see e.g. [10, 11]), it is well known that the asymmetric stretching mode of CO_2 does not quickly equilibrate with the two other modes, especially in the presence of N_2 [1, 4]. The effect of this vibrational non-equilibrium on local radiative properties and spectral distribution of the radiation intensity may be significant.

2. Radiative properties and radiative transfer

2.1. Radiative properties

The radiative transfer equation (RTE) in a gas under nonequilibrium conditions, neglecting scattering, is given by

$$\boldsymbol{u}\cdot\boldsymbol{\nabla}_{\boldsymbol{r}} I_\nu(\boldsymbol{r},\boldsymbol{u}) = \eta_\nu(\boldsymbol{r}) - \kappa_\nu(\boldsymbol{r}) I_\nu(\boldsymbol{r},\boldsymbol{u}) \tag{1}$$

where $I_\nu(\boldsymbol{r},\boldsymbol{u})$ designates the spectral radiative intensity in direction $\boldsymbol{u}$, at point $\boldsymbol{r}$ and wave number ν. $\eta_\nu(\boldsymbol{r})$ and $\kappa_\nu(\boldsymbol{r})$ are the emission and absorption coefficients of the gas at point $\boldsymbol{r}$ and are obtained from a summation over all allowed radiative transitions $u \to l$ between an upper level u and a lower level l of a molecule according to

$$\eta_\nu = \sum_{u\to l} \frac{A_{ul}}{4\pi} hc\nu_{ul} n_u f_{ul}(\nu - \nu_{ul}) \tag{2}$$

$$\kappa_\nu = \sum_{u\to l} (n_l B_{lu} - n_u B_{ul}) h\nu_{ul} f_{ul}(\nu - \nu_{ul}) \tag{3}$$

where n_u and n_l are the populations of levels u and l, A_{ul}, B_{ul}, and B_{lu} are the Einstein coefficients for spontaneous emission, induced emission, and absorption, ν_{ul} is the central wave-number, and $f_{ul}(\nu - \nu_{ul})$ is the spectral line profile (assumed to be the same for the three radiative mechanisms) of the transition $u \to l$; the energy exchange has been approximated by $hc\nu_{ul}$ for each transition $u \to l$.

Spectroscopic data for CO_2 (Einstein coefficients, line positions, collisional broadening parameters) have been taken from the HITEMP-2010 compilation [8], which has been recommended for applications up to 2000 K [12]. The Planck's mean absorption coefficient from HITEMP-2010 is underestimated by about 6% when compared to CDSD4000 [12] at 2500 K. Spectral

line profiles have been modelled as a Voigt function, accounting for Doppler and collisional broadening both evaluated at the rotation/translation temperature T.

The population n_k of any level k involved in the above equations (2,3) is calculated in the framework of the multi-temperature approach used here according to

$$n_k = n_{CO_2} Ab_I \frac{2J_k + 1}{Z_I(T, T_{12}, T_3)} \exp\left(-\frac{E^{rot}\{k\}}{k_b T} - \frac{E^{v_{12}}\{k\}}{k_b T_{12}} - \frac{E^{v_3}\{k\}}{k_b T_3}\right) \quad (4)$$

where n_{CO_2} is the total population of CO_2, Ab_I is the abundance of the isotopologue I considered (only the four main isotopologues have been retained), J_k the quantum number associated to the modulus of the total angular momentum (excluding nuclear spin) of level k. $Z_I(T, T_{12}, T_3)$ is the three temperature partition function of the isotopologue which has been calculated using the approximation of the three uncoupled harmonic oscillators associated to the vibrational modes ν_1, ν_2, ν_3 and of the rigid rotor, whose accuracy was demonstrated at equilibrium in Ref. [13]. $Z_I(T, T_{12}, T_3)$ is given by

$$Z_I(T, T_{12}, T_3) = \frac{k_b T}{2B_I} \times \frac{1}{1 - \exp(-\omega_{1I}/k_b T_{12})} \frac{1}{[1 - \exp(-\omega_{2I}/k_b T_{12})]^2} \frac{1}{1 - \exp(-\omega_{3I}/k_b T_3)} \quad (5)$$

where B_I is the rotational constant of isotopologue I and ω_{1I}, ω_{2I} and ω_{3I} are the vibration energies associated with the three fundamental vibration modes taken for the different isotopologues from Ref. [14].

The notations $E^{rot}\{k\}$, $E^{v_{12}}\{k\}$, and $E^{v_3}\{k\}$ in Eq. (4) introduce a partitioning of the energy $E\{k\}$ of a level k into a rotational part, a vibrational

part associated to the Fermi coupled modes (ν_1, ν_2), and one to the mode ν_3. Most of the upper or lower levels provided in HITEMP-2010 are identified using six quantum numbers v_1, l_2, v_3, r, p, J associated respectively to the modes ν_1, ν_2, ν_3, the index of the level in the Fermi polyad, the parity (e or f) and the total angular momentum. We have retained the quite natural partitioning scheme

$$E^{rot}\{v_1 l_2 v_3 r p J\} = E\{v_1 l_2 v_3 r p J\} - \min_{J'} E\{v_1 l_2 v_3 r p J'\} \quad (6)$$

$$E^{v_3}\{v_1 l_2 v_3 r p J\} = \min_{J'} E\{00 v_3 1 e J'\} \quad (7)$$

$$E^{v_{12}}\{v_1 l_2 v_3 r p J\} = \min_{J'} E\{v_1 l_2 v_3 r p J'\} - E^{v_3}\{v_1 l_2 v_3 r p J\} \quad (8)$$

In the above expressions, the minima over quantum number J' are evaluated considering all the energy levels (upper and lower) identified in HITEMP-2010. The populations of the few non-identified levels have been calculated assuming LTE at temperature T.

2.2. Radiative source terms

The radiative source term in the total energy balance equation is expressed classically as

$$S_R = -\boldsymbol{\nabla}_{\boldsymbol{r}} \cdot \int_\nu \int_{4\pi} I_\nu(\boldsymbol{r}, \boldsymbol{u}) \boldsymbol{u} \mathrm{d}\boldsymbol{u} \mathrm{d}\nu = \int_\nu \int_{4\pi} \left[\kappa_\nu(\boldsymbol{r}) I_\nu(\boldsymbol{r}, \boldsymbol{u}) - \eta_\nu(\boldsymbol{r})\right] \mathrm{d}\boldsymbol{u} \mathrm{d}\nu \quad (9)$$

Einstein coefficients enable to express radiative source terms in population balance equations of each energy level (see e.g. Eq. (13) of Ref. [15]). From these relations, it is quite easy to express the radiative source terms $S_R^{v_{12}}$ and $S_R^{v_3}$ which should appear in the energy balance equation of the vibrational

modes (ν_1, ν_2) and ν_3 respectively, in a similar form to Eq. (9):

$$S_R^{v_{12}/v_3} = \int_\nu \int_{4\pi} \left[\kappa_\nu^{v_{12}/v_3}(\boldsymbol{r}) I_\nu(\boldsymbol{r}, \boldsymbol{u}) - \eta_\nu^{v_{12}/v_3}(\boldsymbol{r})\right] \mathrm{d}\boldsymbol{u}\mathrm{d}\nu \tag{10}$$

where the four new absorption and emission coefficients $\kappa_\nu^{v_{12}}$, $\kappa_\nu^{v_3}$, $\eta_\nu^{v_{12}}$, and $\eta_\nu^{v_3}$ are defined according to

$$\eta_\nu^{v_{12}/v_3} = \sum_{u \to l} \frac{A_{ul}}{4\pi} \Delta E_{ul}^{v_{12}/v_3} n_u f_{ul}(\nu - \nu_{ul}) \tag{11}$$

$$\kappa_\nu^{v_{12}/v_3} = \sum_{u \to l} (n_l B_{lu} - n_u B_{ul}) \frac{\Delta E_{ul}^{v_{12}/v_3}}{c} f_{ul}(\nu - \nu_{ul}) \tag{12}$$

The above expressions are very similar to Eqs. (2,3), where the total energy exchange $hc\nu_{ul}$ associated to the transition $u \to l$ has been replaced by the partial vibrational energy exchanges $\Delta E_{ul}^{v_{12}} = E^{v_{12}}\{u\} - E^{v_{12}}\{l\}$ or $\Delta E_{ul}^{v_3} = E^{v_3}\{u\} - E^{v_3}\{l\}$.

All these source terms can be easily calculated once the spectral RTE Eq. (1) has been solved. The radiative transfer equation is first solved with a line by line approach to get the radiative intensity I_ν, then a second line by line procedure is applied to get the local source terms from the *reduced* emission and absorption coefficients. In the following, all calculations were achieved using a high spectral resolution of 10^{-3} cm^{-1} on the useful spectral domain ranging form 487.5 to 4812.5 cm^{-1}.

3. Collisional relaxation and multi-temperature model

While the calculation of radiative properties relies on accurate rovibrational level energies, the construction of the vibrational multi-temperature model is based on simple harmonic oscillators due to the lack of knowledge

of kinetic rate constants for the high vibrational levels [16]. The energy of a vibrational level $\{i_1, i_2, i_3\}$ is simply given by $\varepsilon_{i_1,i_2,i_3} = i_1\varepsilon_1 + i_2\varepsilon_2 + i_3\varepsilon_3$ with $\varepsilon_k = hc\nu_k$. With the multi-temperature model, vibrational level populations are given by

$$n_{i_1,i_2,i_3}(T_{12}, T_3) = \frac{n_{CO_2}}{Z_{vib}^{CO_2}(T_{12}, T_3)}(i_2+1)\exp\left(-\frac{i_1\varepsilon_1 + i_2\varepsilon_2}{k_B T_{12}}\right)\exp\left(-\frac{i_3\varepsilon_3}{k_B T_3}\right) \tag{13}$$

where the factor $(i_2 + 1)$ results from the degeneracy of the bending mode and the two-temperature vibrational partition function can be factorized as

$$Z_{vib}^{CO_2}(T_{12}, T_3) = Z_{vib}^{12}(T_{12}) Z_{vib}^{3}(T_3) \tag{14}$$

The energy per unit volume stored in each mode associated to each CO_2 vibrational temperature, can then be calculated as

$$E_{vib}^{12} = \frac{n_{CO_2}}{Z_{vib}^{12}(T_{12})}\sum_{i_1,i_2}(i_2+1)(i_1\varepsilon_1 + i_2\varepsilon_2)\exp\left(-\frac{i_1\varepsilon_1 + i_2\varepsilon_2}{k_B T_{12}}\right) \tag{15}$$

$$E_{vib}^{3} = \frac{n_{CO_2}}{Z_{vib}^{3}(T_3)}\sum_{i_3} i_3\varepsilon_3\exp\left(-\frac{i_3\varepsilon_3}{k_B T_3}\right) \tag{16}$$

and simple analytical expressions can be deduced for the two vibrational volumetric heats

$$c_{vib}^{12}(T_{12}) = \frac{\partial E_{vib}^{12}}{\partial T_{12}}, \quad c_{vib}^{3}(T_3) = \frac{\partial E_{vib}^{3}}{\partial T_3} \tag{17}$$

The spatial and temporal evolutions of T_{12} and T_3 depend on the rates of transitions between different vibrational levels due to collisions with different molecules of the mixture. We will consider in the following CO_2-CO-N_2-H_2O-H_2-HCl mixtures representative of high altitude rocket plumes. CO and N_2 will be characterized by two additional vibrational temperatures, T_{CO} and

T_{N_2}, while H_2O and H_2 are assumed to be at LTE at the unique translation-rotation temperature T, due to their short relaxation times. Due to the lack of kinetic data for HCl and to its small concentration in the mixtures considered here, HCl is also assumed to be at equilibrium at T. The relaxation processes considered in this study are summarized in Table 1. They include vibration-translation processes quoted VT_m, m being the involved vibrational mode, and inter-mode vibration-vibration processes quoted $\mathrm{VV}_{mm'}$ (or $\mathrm{VV}_{mm'm''}$) where two (or three) different vibration modes m, m' (m''), eventually for the same species in the case of CO_2, are involved. Here m, m' and m'' belong to the set {1, 2, 3, CO, N2} where 1, 2, and 3 correspond to ν_1, ν_2, and ν_3 CO_2 modes. The intra-mode vibration-vibration processes, where two molecules of the same species exchange one quantum of vibrational energy of the same mode m, are assumed to be sufficiently fast and lead to a Boltzmann distribution inside each mode. For a given collisional process (α) of Table 1 written schematically in the form

$$\text{reaction } \alpha: \qquad A\{i\} + B\{i'\} \underset{K_\alpha^{-1}}{\overset{K_\alpha}{\rightarrow}} A\{i+k\} + B\{i'-k'\} \tag{18}$$

where i, i', $i+k$ and $i'-k'$ designate vibrational levels (single quantum number in the case of CO and N_2, or three vibrational quantum numbers in the case of CO2), the resulting rate of change of vibrational level populations is given by

$$\frac{\mathrm{d}n_{A\{i\}}}{\mathrm{d}t}|_\alpha = \frac{\mathrm{d}n_{B\{i'\}}}{\mathrm{d}t}|_\alpha = K_\alpha^{-1} n_{A\{i+k\}} n_{B\{i'-k'\}} - K_\alpha n_{A\{i\}} n_{B\{i'\}} \tag{19}$$

where K_α and K_α^{-1} are the direct and reverse kinetic rate coefficients. The reverse rate coefficients can be deduced from direct rate coefficients under

Table 1: Vibrational transitions considered in the model

Type	Notation	Reaction
VT	VT_2	$CO_2\{i_1,i_2,i_3\}+M \leftrightarrow CO_2\{i_1,i_2-1,i_3\}+M$
	VT_3	$CO_2\{i_1,i_2,i_3\}+M \leftrightarrow CO_2\{i_1,i_2,i_3-1\}+M$
	VT_{N_2}	$N_2\{i\}+M \leftrightarrow N_2\{i-1\}+M$
	VT_{CO}	$CO\{i\}+M \leftrightarrow CO\{i-1\}+M$
$\mathrm{VV}^M_{CO_2}$	VV_{2-3}	$CO_2\{i_1,i_2,i_3\}+M \leftrightarrow CO_2\{i_1,i_2+3,i_3-1\}+M$
	VV_{1-2-3}	$CO_2\{i_1,i_2,i_3\}+M \leftrightarrow CO_2\{i_1+1,i_2+1,i_3-1\}+M$
VV	VV_{3-N_2}	$CO_2\{i_1,i_2,i_3\}+N_2\{i\} \leftrightarrow CO_2\{i_1,i_2,i_3-1\}+N_2\{i+1\}$
	VV_{3-CO}	$CO_2\{i_1,i_2,i_3\}+CO\{i\} \leftrightarrow CO_2\{i_1,i_2,i_3-1\}+CO\{i+1\}$
	VV_{1-2-CO}	$CO_2\{i_1,i_2,i_3\}+CO\{i\} \leftrightarrow CO_2\{i_1+1,i_2+1,i_3\}+CO\{i-1\}$
	VV_{N_2-CO}	$N_2\{i\}+CO\{i'\} \leftrightarrow N_2\{i-1\}+CO\{i'+1\}$

equilibrium conditions. For instance, if we consider the $\mathrm{VV}^M_{CO_2}$ reaction

$$\mathrm{CO}_2\{i_1,i_2,i_3\}+M \leftrightarrow \mathrm{CO}_2\{i_1,i_2+3,i_3-1\}+M \tag{20}$$

the inverse rate coefficient is given, according to the harmonic oscillator model, by

$$K^M_{\{i_1,i_2,i_3\}\to\{i_1,i_2+3,i_3-1\}}{}^{-1} = K^M_{\{i_1,i_2,i_3\}\to\{i_1,i_2+3,i_3-1\}}\frac{i_2+1}{i_2+4}\exp\left(\frac{3\varepsilon_2-\varepsilon_3}{k_BT}\right) \tag{21}$$

Unfortunately, very few reaction rate coefficients are available in the literature for high lying vibrational levels. Most of experimental studies, like those related to CO_2 lasers, only investigate reactions between lower levels at low temperature. For practical and exhaustive implementation, we use the simple analytical SSH theory [17] that provides, in the framework of harmonic oscillators, a relation between rate coefficients between excited levels and those between low-lying levels. From this theory, we have the following relations [16]:

• For VT exchange

$$K^M_{\{i_3+1\}\to\{i_3\}} = (i_3+1)\, K^M_{\{001\}\to\{000\}} \tag{22}$$

$$K^M_{\{i_2+1\}\to\{i_2\}} = (i_2+1)\, K^M_{\{010\}\to\{000\}} \tag{23}$$

• For VV exchange

$$K^M_{\{i_1,i_2,i_3\}\to\{i_1,i_2+3,i_3-1\}} = \frac{(i_2+1)(i_2+2)(i_2+3)i_3}{3!} K^M_{\{0,0,1\}\to\{0,3,0\}} \tag{24}$$

$$K^M_{\{i_1,i_2,i_3\}\to\{i_1+1,i_2+1,i_3-1\}} = (i_1+1)(i_2+1)i_3\, K^M_{\{0,0,1\}\to\{1,1,0\}} \tag{25}$$

The details of all considered reactions, as well as the literature survey providing the corresponding low-lying level coefficients like $K^M_{\{0,0,1\}\to\{0,3,0\}}$, are given in Appendix A. Further details on the vibrational kinetics can be found in [18].

From the direct and inverse rate coefficients, the population evolution of each vibrational level $\{i\}$ of molecule A can be calculated by summing Eq. (19) over all processes and all the reactions α where this level is involved. The resulting rate of population change is given by

$$R^A_{\{i\}} = \sum_{\text{exchange processes}} \sum_{\text{collider M}} \sum_{\text{reaction } \alpha} \frac{\mathrm{d}n_{A\{i\}}}{\mathrm{d}t}|_\alpha \tag{26}$$

The rate of change of the energy stored in vibrational mode m of molecule A per unit time and unit volume, due solely to collisional processes, is then simply given (in W.m^{-3}) by

$$\frac{\mathrm{d}E^m_{vib}}{\mathrm{d}t} = c^m_{vib}(T_m)\frac{\mathrm{d}T_m}{\mathrm{d}t} = \sum_{\{i\}} \varepsilon^m_{\{i\}} R_{\{i\}} \equiv R_m(T, T_m, T_{m'}...) \tag{27}$$

where $\varepsilon^m_{\{i\}}$ is the energy (J/particle) of vibrational mode m associated with level $\{i\}$.

4. Application to a nozzle expanding flow

4.1. Aero-thermal fields

As a simple application of the previously developed NLTE radiation model, we consider a quasi-unidimensional expanding isentropic flow in a conical nozzle of radius R=10 cm at the throat and a cone angle of 15 degrees. The flowing gas is a non-reacting perfect mixture of N_2-CO_2-H_2O with respective molar fractions of 70%, 20% and 10%. The flow conditions at the throat are assumed to be sonic (Mach=1) with an initial LTE temperature $T_0 = 3000$ K, a mass flow rate of 9 kg.m^{-2}.s^{-1}, leading to an initial velocity $u_0 = 1118$ m.s^{-1}. The LTE one-dimensional density (ρ), velocity (u), temperature (T), and pressure (p) fields are calculated from the integration along the nozzle axis x of conservation equations of mass, momentum and total energy

$$\frac{\mathrm{d}}{\mathrm{d}x}(\rho u A) = 0;\ \rho u\frac{\mathrm{d}u}{\mathrm{d}x} + \frac{\mathrm{d}p}{\mathrm{d}x} = 0;\ c_p\frac{\mathrm{d}T}{\mathrm{d}x} + u\frac{\mathrm{d}u}{\mathrm{d}x} = 0 \tag{28}$$

where $A(x)$ is the nozzle cross section, c_p the specific total heat at constant pressure, and from the isentropic relation $\frac{\mathrm{d}p}{p} = \gamma\frac{\mathrm{d}\rho}{\rho}$. The results of this integration are shown in Fig. 1 (left). It is assumed as a first approach that vibrational disequilibrium does not affect the obtained macroscopic variables. Vibrational temperatures are therefore calculated by post-processing these fields and by replacing $\frac{\mathrm{d}T_m}{\mathrm{d}t}$ by $u(x)\frac{\mathrm{d}T_m}{\mathrm{d}x}$ in Eq. (27). Figure 1 (right) shows a strong imbalance between translation-rotation temperature T and vibrational temperatures T_m. CO_2 (12) mode temperature is closer to T due to faster vibration-translation relaxation for this mode. We can notice also that the temperature of mode (3) of CO_2 remains close to that of the vibration mode

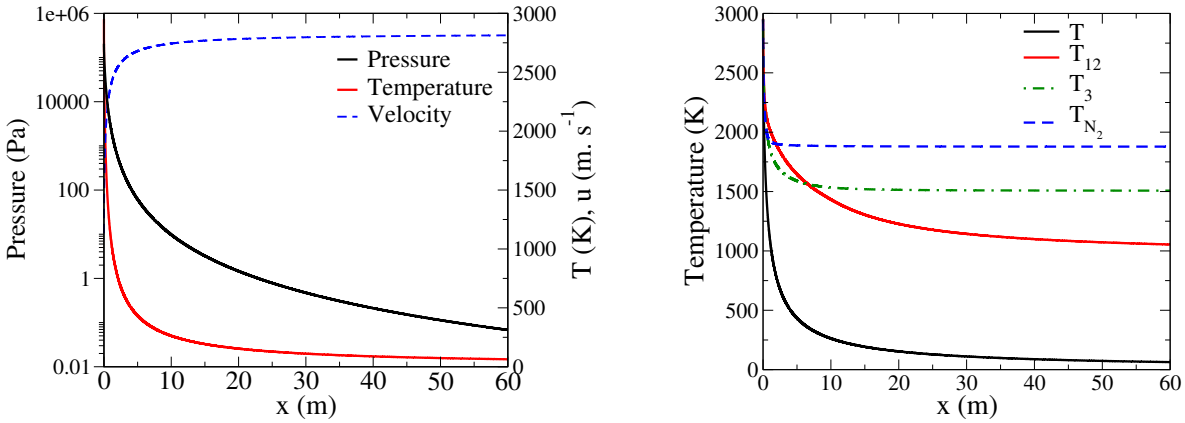

Figure 1: Left: Pressure, temperature and velocity along the nozzle axis. Right: Same translation-rotation temperature T, and vibrational temperatures.

of N_2 due to close vibration frequencies. Figure 2 shows the absorption and emission spectra of CO_2 computed from the line by line approach presented in Sec. 2 and the computed values of T, T_{12} and T_3, at a distance x =2 m from the nozzle throat. The high resolution spectra are convolved with a rectangular window of 25 cm^{-1} width for legibility reasons. At x =2 m, the values of T, T_{12} and T_3 are 771, 1889 and 1719 K respectively. Compared to equilibrium calculations at temperature T, the absorption coefficient in the ν_3 region is significantly shifted towards smaller wave numbers due to anharmonicity and the over-population of high vibrational levels. Let us recall that level populations and line positions in radiation calculations are based on the actual level energies and not on the uncoupled harmonic oscillator model. This over-population also leads to a much stronger emission as shown on the right part of Fig. 2. While the ratio $\eta_\sigma/\kappa_\sigma$ at LTE is the smooth Planck's function at the considered equilibrium temperature, Fig. 3 shows an erratic behaviour of this ratio under nonequilibrium conditions. In the significantly

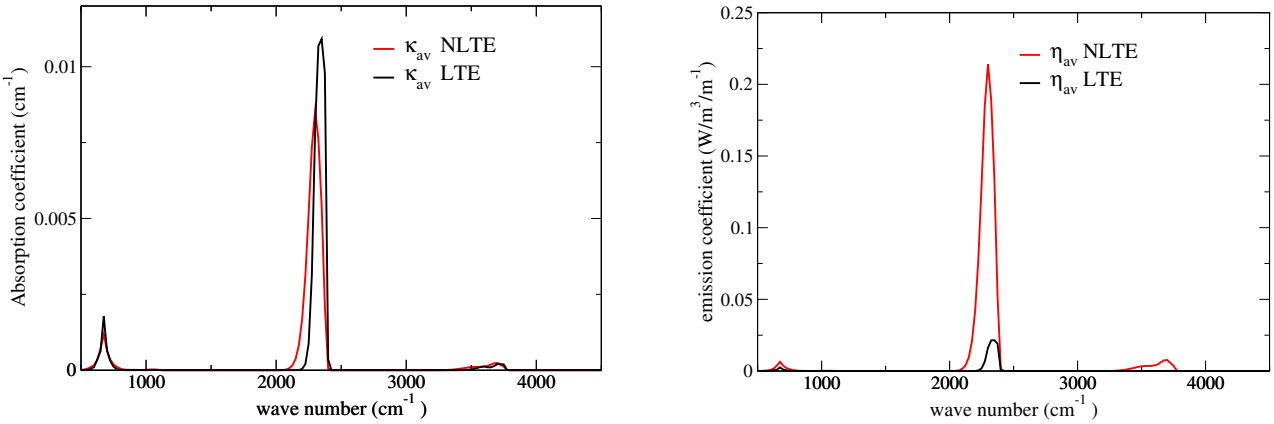

Figure 2: Absorption (left) and emission (right) coefficients calculated at LTE and NLTE at a distance x =2 m from the nozzle throat. Line by line results are averaged over 25 cm^{-1} for legibility.

absorbing and emitting regions of the spectrum, it remains bounded by the Planck functions at the two vibrational temperatures of CO_2. However, for nearly transparent regions dominated by far line wings and weak transitions involving very high rotational levels, this ratio can take values outside the Planck's functions at the two temperatures T_{12} and T_3.

4.2. Radiative transfer

The RTE Eq. (1) has been solved along the nozzle axis with radiative properties obtained from the nonequilibrium thermal fields presented above, and assuming no incoming intensity at the throat of the nozzle. The resulting spectral intensity at the abscissa $x = 60$ m is shown in the left part of Fig. 4, and compared to the results obtained assuming LTE along the column at translation/rotation temperature. The high resolution spectral distribution of these intensities has been averaged on bands of width 25 cm^{-1} in order to make comparisons easier. A strong increase of the outgoing intensity is

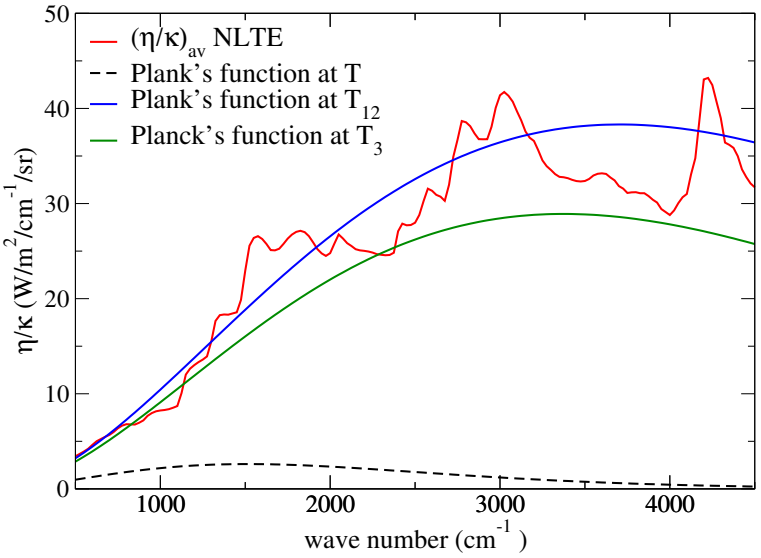

Figure 3: Emission to absorption coefficient ratio and Planck's functions at the three temperatures at x =2 m. Line by line ratios are averaged over 25 cm^{-1} for legibility.

observed when vibrational disequilibrium is accounted for, due to the "hot freezing" of the vibrational temperatures T_{12} and T_3 along the expanding flow. The total intensity increases from 11.5 at LTE to 17 kWm^{2}sr^{-1} at NLTE.

In order to estimate radiative source terms and fluxes, we consider an academic 1D planar geometry whose radiative properties vary along the normal to the slab as those of the above expanding flow along the nozzle axis. The total thickness of the slab is $L = 60$ m, corresponding to the maximum abscissa considered in the above flow expansion calculation. We consider no incoming intensity and no reflection at the boundaries of the slab. The spectral radiative flux incident on the low pressure boundary at abscissa $x = L$

can be easily calculated according to

$$q_\nu(x=L) = 2\pi \int_0^{c_\nu^L} \frac{\eta_\nu}{\kappa_\nu}(c_\nu) E_2(c_\nu^L - c_\nu) \mathrm{d}c_\nu \tag{29}$$

where the current optical depth $c_\nu = \int_0^x \kappa_\nu(x')\mathrm{d}x'$ varies from 0 at x =0 to c_ν^L at $x = L$. In a similar way, the spectral incoming intensity at a current abscissa x is obtained from

$$\mathcal{G}_\nu(x) \equiv \int_{4\pi} I_\nu(x, \boldsymbol{u})\mathrm{d}\boldsymbol{u} = 2\pi \int_0^{c_\nu^L} \frac{\eta_\nu}{\kappa_\nu}(c'_\nu) E_1(|c_\nu - c'_\nu|)\mathrm{d}c'_\nu \tag{30}$$

In the above expressions, E_1 and E_2 designates the usual exponential-integral functions [19]. The three energy radiative source terms defined in Eqs. (9,10) can be expressed from this incoming intensity according to

$$S_R(x) = \int_\nu \left[\kappa_\nu(x)\mathcal{G}_\nu(x) - 4\pi\,\eta_\nu(x)\right] \mathrm{d}\nu \tag{31}$$

$$S_R^{v_{12}/v_3}(x) = \int_\nu \left[\kappa_\nu^{v_{12}/v_3}(x)\mathcal{G}_\nu(x) - 4\pi\,\eta_\nu^{v_{12}/v_3}(x)\right] \mathrm{d}\nu \tag{32}$$

$$\tag{33}$$

The spectral radiative flux calculated at the boundary $x = L$ is shown on the right part of Fig. 4, accounting for vibrational disequilibrium or not. Its spectral structure is very similar to that of the intensity on the nozzle axis (left part of the figure). The total radiative flux is increased by about 50 % when vibrational disequilibrium is accounted for. The three radiative source terms $-S_R$, $-S_R^{v_{12}}$, and $-S_R^{v_3}$ are respectively compared in Fig. 5 to $-\rho c_p u \mathrm{d}T/\mathrm{d}x$, $-c_{vibr}^{v_{12}} u \mathrm{d}T_{12}/\mathrm{d}x$, and $-c_{vibr}^{v_3} u \mathrm{d}T_3/\mathrm{d}x$, which are the left members of the balance equations where they should appear. Radiative source terms appear several orders of magnitude lower than non-radiative ones, justifying *a posteriori* the non coupled approach of radiative transfer. In a similar way,

vibrational energy variations are much smaller than total enthalpy ones, justifying also the post-processing treatment of vibrational disequilibrium. Let note that the radiative source term related to the ν_3 mode contains the main part of the total radiative source term.

We can conclude for this application that radiative source terms may be neglected in total and partial energy balance equations and uncoupled flow field calculations are justified. However, radiation level itself is significantly affected by vibrational nonequilibrium.

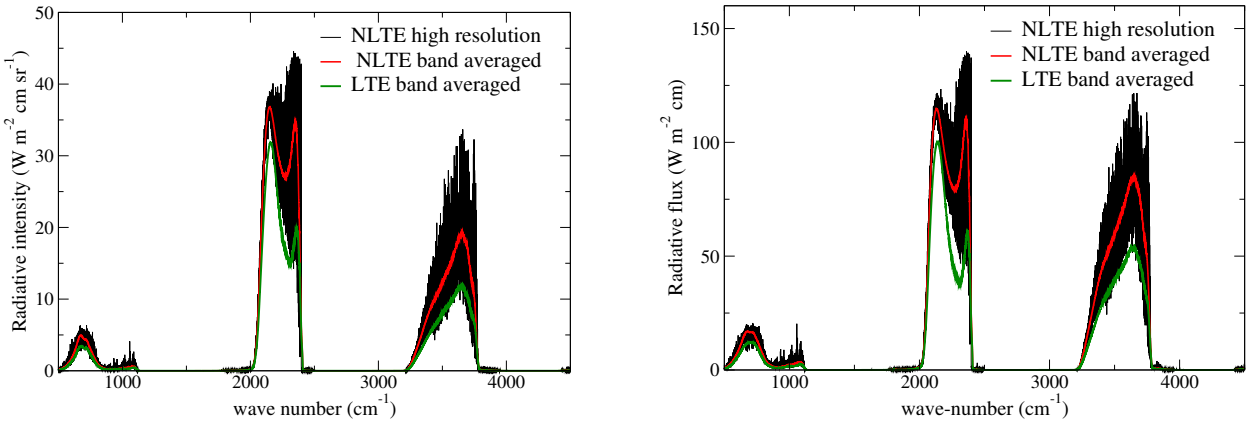

Figure 4: Left: Spectral radiative intensity along the nozzle axis at a distance $x = 60$ m from the throat. Right: Spectral radiative flux in 1D slab configuration at the same location.

5. Application to a high-altitude rocket plume

The nonequilibrium model is applied in this section to the computation of CO_2 radiation emission along selected lines of sight in the plume of a high altitude rocket engine. The simulated case is that of the "Bow Shock Ultraviolet 2" (BSUV2) experiment [20], and more specifically, the plume of

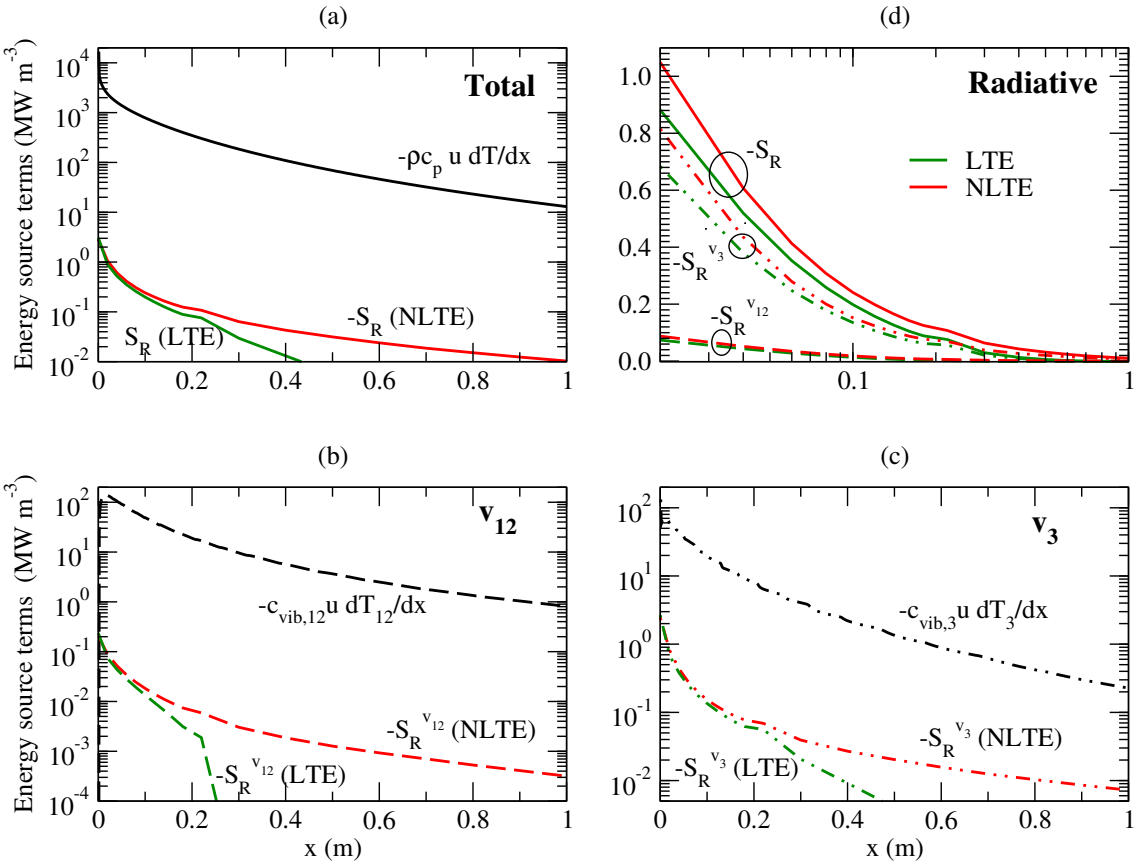

Figure 5: Energy radiative source terms $-S_R$, $-S_R^{v_{12}}$, and $-S_R^{v_3}$ considering NLTE (red) or LTE (green), compared to non radiative terms (black). The three radiative source terms at NLTE and LTE are gathered in part (d) for inter-comparisons.

the solid propellant motor Antares II corresponding to the second stage of the rocket. This rocket was launched in 1991 at an altitude of 109.6 km and measurements of spectral radiation from the plume were obtained in the UV range from 0.2 to 0.4 μm. The main dimensions of Antares II motor are shown in Fig. 6.

At the nozzle exit, the mixture contained about 37.5 % mass fraction of

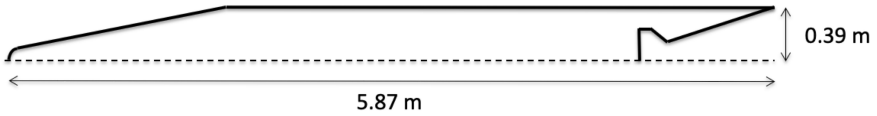

Figure 6: Scheme of Antares II rocket of the BSUV2 experiment.

alumina particles resulting from the combustion of aluminum incorporated in the solid propellant. The gaseous phase was a mixture of CO_2, CO, H_2O, HCl, N_2, H_2 and H with respective mass fractions of 0.0304, 0.6235, 0.0492, 0.0352, 0.230, 0.0314, and 3 10^{-4}. Due to its small concentration, atomic hydrogen is neglected in vibration relaxation processes.

In a previous study [21], we have simulated numerically the flow and thermal fields of the plume, coupled to radiation, under gas local thermodynamic equilibrium assumption. Thermal nonequilibrium between the gaseous phase and several classes of particles of different sizes, considered at different temperatures, was however modelled. It was shown that radiation was dominated by alumina particles in this application, though gas radiation, and notably CO_2 emission in the 4.3 μm region, was not negligible. It was also shown that radiation cooling of alumina particles was an important mechanism to explain the radiation measurements in the UV range. However, the direct feedback of radiative transfer on gas temperature field was found negligible. More details on the modelling, computational methods, and main results of these numerical simulations are given in [18, 21]. The resulting gas temperature and pressure fields are shown in Fig. 7.

The aim of the present section is to analyse vibrational nonequilibrium ef-

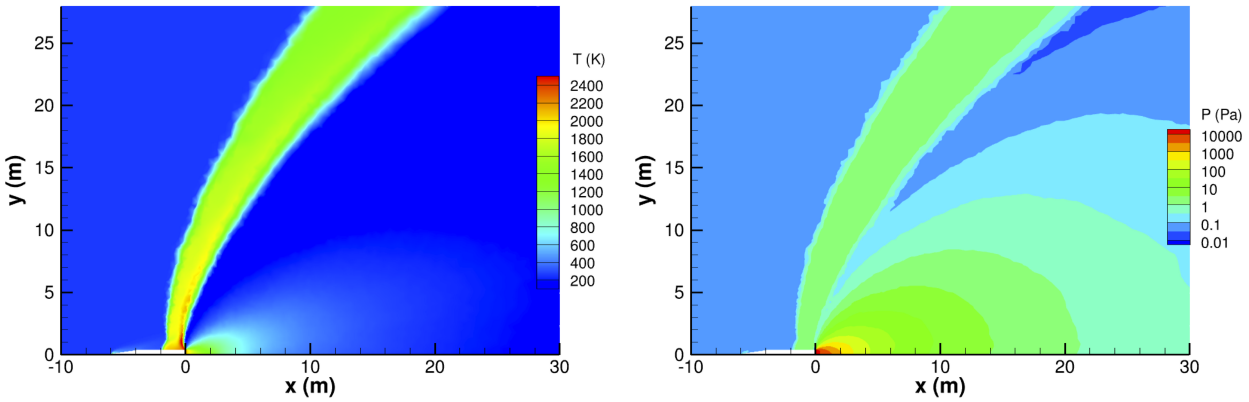

Figure 7: Gas temperature (left) and pressure (right) calculated under gas LTE assumption.

fects on CO_2 radiation under realistic conditions corresponding to the plume of Antares II motor. Although gas radiation can be neglected in the gas-phase energy balance equation as compared to expansion thermodynamic cooling, an accurate estimation of gas emission may be important for the signature of the plume. We assume in a first approach that, as for the previous nozzle flow, the vibrational nonequilibrium would not significantly affect macroscopic quantities such as the translation temperature, pressure and velocity fields. We also assume that, due to its fast relaxation times, H_2O molecules are at equilibrium with translation and rotation. The multi-temperature model comprises a translation temperature T, two vibrational temperatures T_{12} and T_3 for CO_2, and two supplementary vibrational temperatures T_{CO} and T_{N2} respectively for CO and N_2. Owing to their small mass fractions (3.5% and 3.1% for HCl and H_2 respectively), and to the lack of vibrational kinetic data for HCl, these two molecules are also assumed at local equilibrium at the translation-rotation temperature. As found for the

planar geometry considered in Sec. 4, the radiative source terms in the vibrational energy equations are assumed to be negligible in comparison with other terms.

From the above assumptions, a post-processing method of the fields obtained at LTE is employed to determine the fields of all vibrational temperatures. A Lagrangian method is developed to reconstruct the local vibrational temperatures from a large number of trajectories. The trajectories are launched from the different inflow sections including the exit section of the rocket nozzle and the upstream external atmosphere. For each molecular species M, the unit vector $\boldsymbol{n}_M$ along the trajectory is calculated such that

$$\boldsymbol{n}_M \times (\boldsymbol{u} + \boldsymbol{V}_M) = 0 \tag{34}$$

where $\boldsymbol{u}$ is the hydrodynamic velocity vector and $\boldsymbol{V}_M$ is the molecular diffusion velocity of species M. The diffusion velocity is calculated from the gradient of the mass fraction of species M through Fick's law, as explained in Ref. [21]. Accounting for diffusion velocities is particularly important in the region close to the shock where the N_2 molecules coming from the outer atmosphere are mixed with those issued from the nozzle jet. Along each trajectory of abscissa s, the vibrational temperature of a given mode m is calculated according to

$$c^m_{vib}(T_m)\, v_m(s) \frac{\partial T_m}{\partial s} = R_m(T, T_{12}, T_3, T_{N_2}, T_{CO}, n_{CO_2}, n_{N_2}, n_{H_2O}, n_{CO}, n_{H2}) \tag{35}$$

where $v_m = \| \boldsymbol{u} + \boldsymbol{V}_M \|$ is the modulus of the velocity of species M associated with vibrational mode m. These equations are solved iteratively in a coupled manner in order to take into account possible crossing of trajectories

of different species, mainly due to outer atmospheric N_2 molecules. Indeed, when for instance a CO_2 trajectory crosses a N_2 trajectory in the shock layer, the source terms of Eq. (35) for CO_2 modes and for N_2 mode both need the solutions along the two trajectories. In practice, a regular mesh is introduced and the local vibrational temperatures in each cell are computed from the arithmetic mean of the temperatures issued from all points and all trajectories crossing this cell. Figures 8 and 9 show the difference between vibrational temperatures and translation-rotation temperature for CO and N_2, and for modes (12) and (3) of CO_2, respectively.

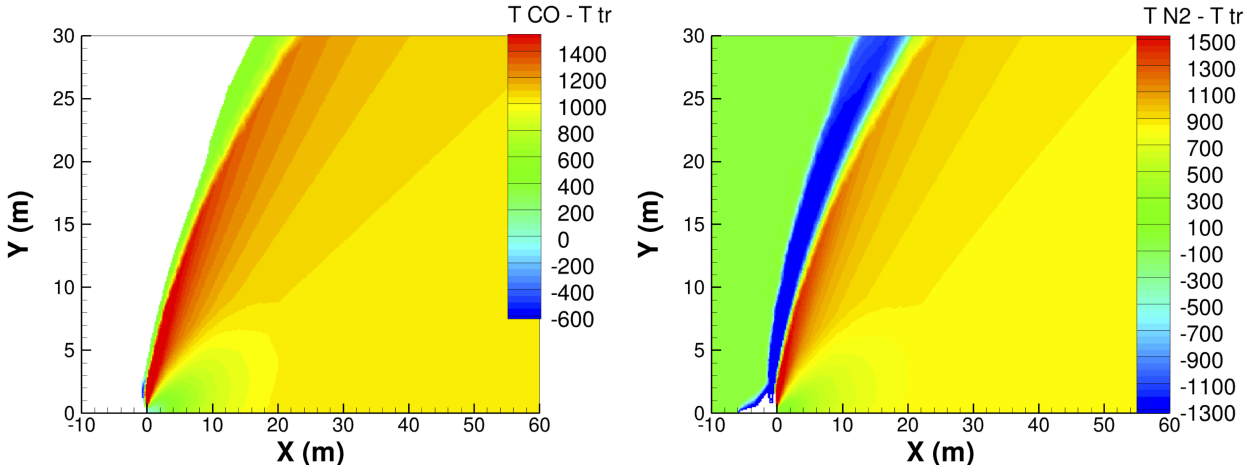

Figure 8: Departure from equilibrium for vibrational modes of CO and N_2.

We first notice the strong disequilibrium of CO and N_2 vibration modes and of the antisymmetric CO_2 mode in the jet, the temperature differences being of the order of 700 to 1000 K at the core of the jet after relaxation ($X > 20$ m). The disequilibrium is more marked when approaching the shock, the density decreasing strongly. The disequilibrium of the symmetrical and transverse modes of CO_2 is meanwhile less important (because of the

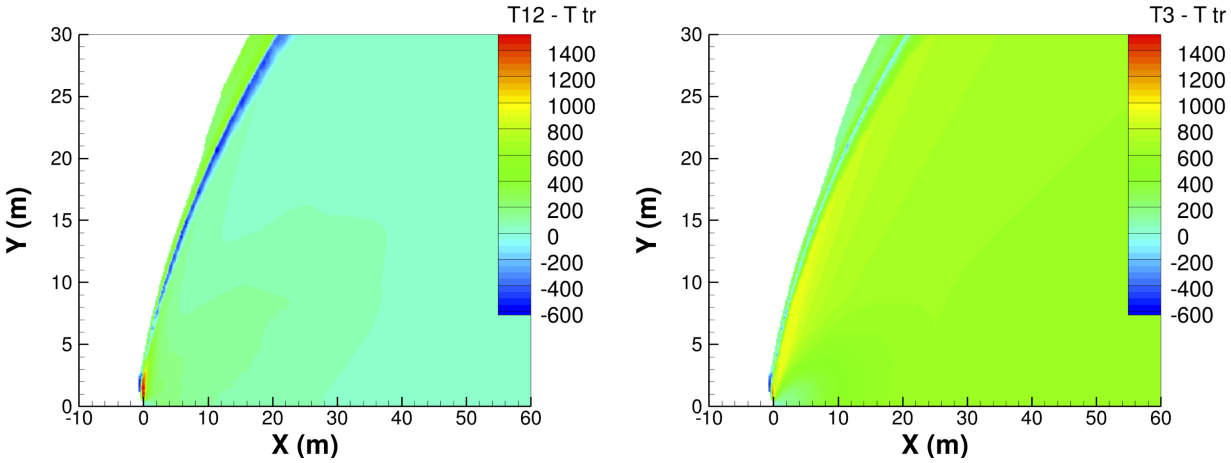

Figure 9: Departure from vibrational equilibrium for modes 12 and 3 of CO_2.

fast Vibration/Translation exchanges), the difference $T_{12} - T$ varying from 400 K at the beginning of the expansion to about 100 K at the end of the expansion.

N_2 molecules from the atmosphere undergo an inverse disequilibrium due to compression in the shock. The modes of vibration are indeed in equilibrium with the translation until the shock. There, the translation temperature increases strongly and the vibration mode of N_2 remains weakly excited (zone shown in dark blue in Fig. 8). The vibration temperature increases towards the translation temperature as the molecules pass through the shock, where the increasing abundance of H_2 and H_2O molecules enhance Vibration/Translation exchanges.

Radiative intensities have been computed along some lines of sight from the vibrational temperature fields obtained with the Lagrangian method. Two columns have been considered. The first column is 20 m long, starts from the nozzle exit at $Y = r/2$ where r is the nozzle radius at nozzle exit,

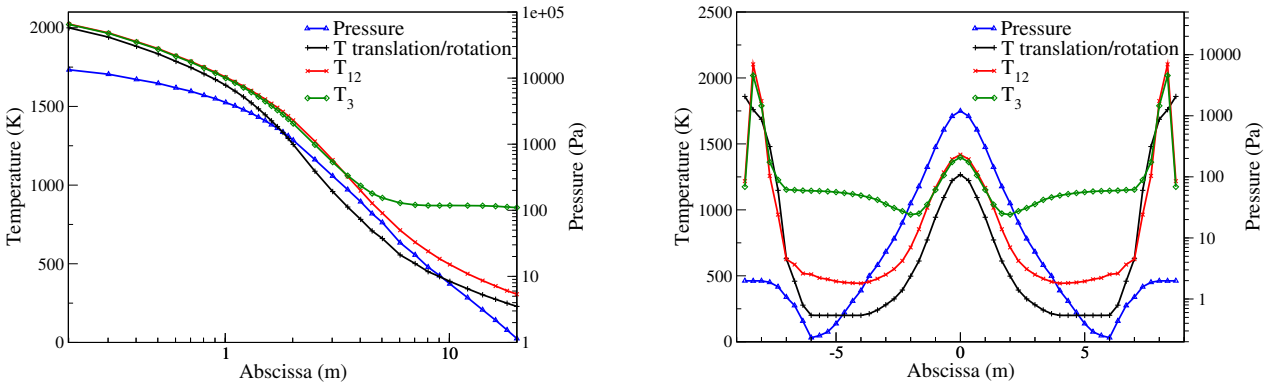

Figure 10: Temperature and pressure distributions along the axial (left) and transverse (right) lines of sight.

and is parallel to the plume axis of symmetry. It is called hereafter axial column. The second column, called transverse column, crosses the plume perpendicularly to its axis and intersects this axis at $X = 2$ m away from the nozzle exit. Pressure and temperature distributions along these columns are plotted on Fig. 10. The disequilibrium is relatively weak along the axial column even if it becomes significant for the antisymmetric stretching mode of CO_2 for $X > 6$ m. However, in this region, the pressure is very weak and its contribution to emission or absorption is expected to be very small. More important differences between vibrational temperatures and the translation/rotation temperature are observed for the transverse column.

Figure 11 displays the radiative intensities escaping from the two columns in the spectral range 1900–2500 cm^{-1}. The high resolution spectra are convolved with a rectangular window of 5 cm^{-1} width. For the axial column, the escaping intensity is computed at $X = 20$ m in the direction opposite to the nozzle. As could be expected from pressure and temperature distri-

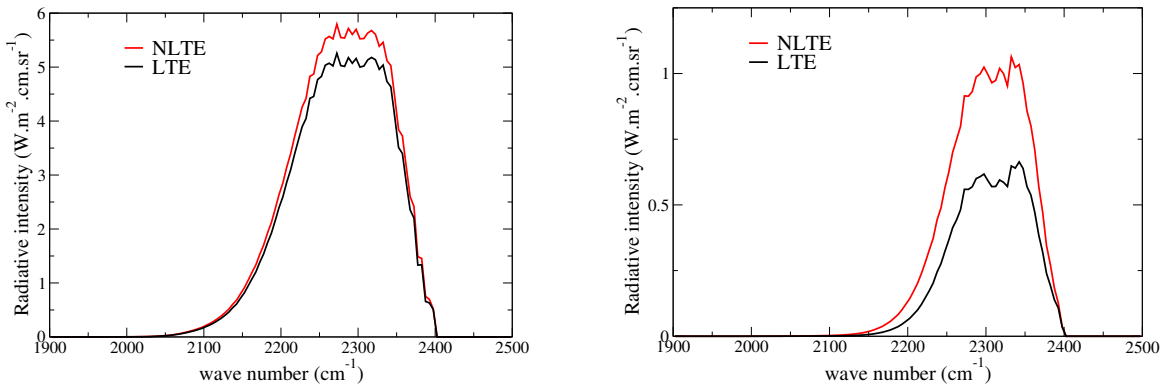

Figure 11: Radiative intensities at the exit of the axial (left) and transverse (right) lines of sight. Line by line results are averaged over 5 cm^{-1} for legibility.

butions shown in Fig. 10, vibrational nonequilibrium effects on the escaping intensities are stronger for the transverse column. The integrated intensity over all the band is increased for this line of sight from 80 to 135 Wm^{-2}Sr^{-1} due to the partial "freeze" of CO_2 vibration modes, and especially of the antisymmetric stretching mode.

6. Conclusion

A consistent model is developed in this work for the prediction of CO_2 radiation under vibrational nonequilibrium conditions in the framework of multi-temperature thermodynamic description of the medium. The evolution of vibrational temperatures is determined from a detailed collisional vibration specific model. Line-by-line calculations are based on level populations deduced from the three temperatures T, T_{12} and T_3, and in turn, partial absorption and emission coefficients allowed us to derive the radiative source terms to be included in the multi-temperature balance equations. The developed model can be applied to several problems including for instance Mars

atmospheric entries. In this work two applications are investigated. A first application to the case of an expanding flow in a conical nozzle shows that the partial freeze of vibration excitation may significantly increase radiative intensities. Based on the aero-thermal fields obtained for this conical nozzle, the full radiative transfer calculations are carried out in the academic planar medium case. This academic geometry is useful for the quantitative determination of radiative fluxes and total and partial radiative source terms. It is found that, for the considered application, both total and partial radiative source terms are negligible compared to the expansion terms, which justifies the non-coupled calculations. The second application considers the plume of the high altitude Antares II motor of the BSUV2 experiment. Based on previous calculations of the flow and temperature fields at local thermodynamic equilibrium of the gas phase, a Lagrangian method was employed to post-process these fields and to predict vibrational temperature distributions. Differences up to 1000 K between vibrational temperatures and the translation-rotation temperature are found, which leads to a more or less strong enhancement of radiation escaping from the plume, depending on the considered line of sight.

Due to the very large CPU time and/or storage capability requirements, radiation calculations in the case of the rocket plume were limited to some chosen lines of sight in the plume. Full calculations of radiative fluxes and source terms would require the development of specific approximate models, like the statistical narrow-band model, which will be explored in future work.

Acknowledgments This work was performed using HPC resources from GENCI-IDRIS (Grant 2019- A0062B00209).

Appendix A: Vibrational kinetic constants

We present in this appendix the different formulations of kinetic constants employed for vibrational relaxation calculations. Literature survey provided the expressions of kinetic constants k, expressed in $\mathrm{Pa}^{-1}.\mathrm{s}^{-1}$ (or $\mathrm{atm}^{-1}.\mathrm{s}^{-1}$), or K, expressed in $\mathrm{m}^3.\mathrm{part}^{-1}.\mathrm{s}^{-1}$, for the relaxation of the first vibrational levels. The relation between k and K is given by $K = k \times k_B T$. We list below the set of all expressions used in this study, gathered in different tables according to the employed formula for temperature dependence. Note that the effects of VT_3 process were found negligible as in [22] and are not included here. An asterix added to a reference number means that the coefficients a_i of the analytical expressions were adjusted in this work to fit the experimental kinetic constants given in that reference.

Table 2: Expressions in the form $\log_{10}(K) = \sum_{i=0}^{2} a_i T^{-\frac{i}{3}}$, with K in $\mathrm{m}^3.\mathrm{part}^{-1}.\mathrm{s}^{-1}$.

Reaction	molecule M	a_0	a_1	a_2	reference
VT_2: $CO_2\{0,1,0\} + M \rightarrow CO_2\{0,0,0\} + M$	CO_2	-13.07	-83.28	220.3	[23]*
	N_2	-13.75	-83.97	223	[23]*
	H_2	-18.1	3.67	0	[23]*
	H_2O	-18.64	11.74	0	[23]*
VT_{N_2} : $N_2\{1\} + M \leftrightarrow N_2\{0\} + M$	N_2, CO_2, CO	-11.72	-123.9	0	[23]*
	H_2	-16.12	-31.12	0	[23]*
	H_2O	-13.25	-53	0	[23]*
VV_{2-3} : $CO_2\{0,0,1\} + M \rightarrow CO_2\{0,3,0\} + M$	CO_2	-11.9	-102.9	304.5	[23]*
	N_2	-9.54	-144.06	462.1	[23]*
	H_2O	-21.3	42.29	-147.5	[23]*

Table 3: Expressions in the form $\log_{10}(K) = \sum_{i=0}^{2} a_i T^{-i}$, with K in $\mathrm{m^3.part^{-1}.s^{-1}}$.

Reaction	a_0	a_1	a_2	reference
VV_{3-N_2}: $CO_2\{0,0,1\} + N_2\{0\} \rightarrow CO_2\{0,0,0\} + N_2\{1\}$	-18.2	-8.10^{-4}	4.10^{-7}	[23]*

Table 4: Expressions in the form $\log_{10}(k) = \sum_{i=0}^{2} a_i T^{-\frac{i}{3}}$, with k in $\mathrm{atm^{-1}.s^{-1}}$.

Reaction	molecule M	a_0	a_1	a_2	reference
VT_{CO} : $CO\{1\} + M \rightarrow CO\{0\} + M$	N_2, CO_2, CO	12.820	-155.91	450.5	[24]
VT_{CO} : $CO\{1\} + M \rightarrow CO\{0\} + M$	H_2	11.372	-78.32	192.73	[25]*
VV_{1-2-3} : $CO_2\{0,0,1\} + M \rightarrow CO_2\{1,1,0\} + M$	CO_2, CO, N_2	12.662	-88.87	272.5	[24]
VV_{1-2-CO} : $CO_2\{1,1,0\} + CO\{0\} \rightarrow CO_2\{0,0,0\} + CO\{1\}$		10.708	-69.94	203.3	[24]
VV_{2-CO} : $CO_2\{0,3,0\} + CO\{0\} \rightarrow CO_2\{0,0,0\} + CO\{1\}$		10.708	-69.94	203.3	[24]
VV_{3-CO} : $CO_2\{0,0,1\} + CO\{0\} \rightarrow CO_2\{0,0,0\} + CO\{1\}$		9.144	-31.91	-103.5	[24]
VV_{N_2-CO} : $N_2\{1\} + CO\{0\} \rightarrow N_2\{0\} + CO\{1\}$		7.002	-11.53	0	[26]*

Table 5: Expressions in the form $\log_{10}(k) = \sum_{i=0}^{3} a_i T^{-\frac{i}{3}}$, with k in $\mathrm{atm^{-1}.s^{-1}}$.

Reaction	molecule M	a_0	a_1	a_2	a_3	reference
VV_{2-3} : $CO_2\{0,0,1\} + M \rightarrow CO_2\{0,3,0\} + M$	H_2	16.315	-199.4	1356	-3081	[27]*

References

[1] F. S. Simmons, Rocket Exhaust Plume Phenomenology, The Aeroscpace Press, 2000.

[2] E. Kustova, E. Nagnibeda, Y. Shevelev, N. Syzranova, Comparison of different models for non-equilibrium CO_2 flows in a shock layer near a blunt body, Shock Waves 21 (2011) 273–287.

[3] C. Patel, Continuous-wave laser action on vibrational-rotational transitions of CO_2, Physical Review 136 (1964) A1187–A1194.

[4] J. D. Anderson, Gasdynamic Lasers: An Introduction, Academic Press, 1976.

[5] M. Lopes-Puertas, G. Zaragoza, M. A. Lopez-Valverde, Non local thermodynamic equilibrium (LTE) atmospheric limb emission at 4.6 μm 1. An update of the CO_2 non-LTE radiative transfer model, Journal of Geophysical Research 103 (1998) 8499–8513.

[6] M. Lopes-Puertas, R. Rodrigo, J. J. Lopez-Moreno, F. W. Taylor, A non-LTE radiative transfer model for infrared bands in the middle atmosphere. II.CO_2 (2.7 and 4.3 μm) and water vapour (6.3 μm) bands and N_2 (1) and O_2 (1) vibrational levels, Journal of Atmospheric and Terrestrial Physics 48 (1986) 749–764.

[7] E. Nagnibeda, E. Kustova, Non-Equilibrium Reacting Gas Flows. Kinetic Theory of Transport and Relaxation Processes, Springer, 2009.

[8] L. S. Rothman, I. E. Gordon, R. J. Barber, H. Dothe, R. R. Gamache, A. Goldman, V. I. Perevalov, S. A. Tashkun, J. Tennyson, HITEMP, the high-temperature molecular spectroscopic database, Journal of Quantitative Spectroscopy and Radiative Transfer 111 (15) (2010) 2139–2150.

[9] G. Herzberg, Molecular spectra and molecular structure. II. Infrared and Raman Spectra of polyatomic molecules, Van Nostrand Company, 1956.

[10] P. A. Gnoffo, R. Gupta, J. Shinn, Conservation equations and physical models for hypersonic air flows in thermal and chemical nonequilibrium, Technical Paper 2867, NASA Langley Research Center (Feb 1989).

[11] C. Park, J. T. Howe, R. L. Jaffe, G. V. Candler, Review of Chemical-Kinetic Problems of Future NASA Missions, II: Mars Entries, Journal of Thermophysics and Heat Transfer 8 (1) (1994) 9–23.

[12] S. A. Tashkun, V. I. Perevalov, CDSD-4000: High-resolution, high-temperature carbon dioxide spectroscopic databank, Journal of Quantitative Spectroscopy and Radiative Transfer 112 (9) (2011) 1403–1410.

[13] S. Depraz, M. Y. Perrin, P. Rivière, A. Soufiani, Infrared emission spectroscopy of CO2 at high temperature. Part II: Experimental results and comparisons with spectroscopic databases, Journal of Quantitative Spectroscopy and Radiative Transfer 113 (1) (2012) 14–25.

[14] A. Chedin, The carbon dioxide molecule: Potential, spectroscopic, and molecular constants from its infrared spectrum, Journal of Molecular Spectroscopy 76 (1) (1979) 430–491.

[15] B. Lopez, M. Y. Perrin, Ph. Rivière, A. Soufiani, Coupled Nonequilibrium Flowfield-Radiative Transfer Calculation Behind a Shock Wave, Journal of Thermophysics and Heat Transfer 27 (3) (2013) 404–413.

[16] E. Kustova, E. Nagnibeda, On a correct description of a multi-temperature dissociating CO_2 flow, Chemical Physics 321 (2006) 293–310.

[17] R. Schwartz, Z. Slawsky, K. Herzfeld, Calculation of vibrational relaxation times in gases, The Journal of Chemical Physics 20 (1952) 1591–1599.

[18] Q. Binauld, Simulation et modélisation du rayonnement dans les jets de moteurs à propergol solide à haute altitude, Ph.D. thesis, University Paris Saclay, CentraleSupélec (2018).

[19] M. F. Modest, Radiative heat transfer, 3rd Edition, Academic Press, 2013.

[20] P. W. Erdman, E. Zipf, P. Espy, C. Howlett, D. A. Levin, G. V. Candler, In-situ measurements of UV and VUV radiation from a rocket plume and re-entry bow shock, AIAA paper (92-0124).

[21] Q. Binauld, J. M. Lamet, L. Tessé, P. Rivière, A. Soufiani, Numerical simulation of radiation in high altitude solid propellant rocket plumes, Acta Astronautica 158 (2019) 351–360.

[22] I. Armenise, E. Kustova, Mechanisms of Coupled Vibrational Relaxation and Dissociation in Carbon Dioxide, Journal of Physical Chemistry A 122 (23) (2018) 5107–5120.

[23] R. L. Taylor, S. Bitterman, Survey of vibrational relaxation data for processes important in the CO_2-N_2 laser system, Reviews of Modern Physics 41 (1) (1969) 26–47.

[24] O. Achasov, D. Ragosin, Rate constants of VV exchange for CO2-GDL, Preprint 16 (Institute of Heat and Mass Transfer, Minsk, Bielarus), 1986, as reported in [28].

[25] D. J. Miller, R. C. Millikan, Vibrational relaxation of carbon monoxide by hydrogen and helium down to 100 K, The Journal of Chemical Physics 53 (8) (1970) 3384–3385.

[26] C. W. von Rosenberg Jr, K. Bray, N. H. Pratt, Shock tube vibrational relaxation measurements: N_2 relaxation by H_2O and the CO–N_2 V-V rate, The Journal of Chemical Physics 56 (7) (1972) 3230–3237.

[27] V. V. Nevdakh, L. N. Orlov, N. S. Leshenyuk, Temperature dependence of the vibrational relaxation rate constants of CO_2 (00^01) in binary mixtures, Journal of Applied Spectroscopy 70 (2) (2003) 276–284.

[28] E. Kustova, E. Nagnibeda, I. Armenise, Vibrational-Chemical Kinetics in Mars Entry Problems, The Open Plasma Physics Journal 7 (Suppl 1: M5) (2014) 76–87.